InceptionV3 model, and its pre-training weights were obtained to build an InceptionV3 network model combined with migration learning, which improved the recognition accuracy by 1.2 percentage points over InceptionV3 and took 5 s faster per round of iteration on average. Then, the global average pooling layer is used to replace the spreading layer after the convolutional layer in the InceptionV3 network, and the reduced dimensional 1, 3, 5, 6, 7, 8, 9, 10 layers feature information is fused using concat, and the relu activation function and Dropout layer are used to reduce the degree of network overfitting. model. Separation experiments show that the recognition rate of individual beef cattle with the improved InceptionV3 model is improved by 4.1 percentage points.

Summary and Prospect. Agriculture and animal husbandry are the basic guarantee of China's people's livelihood and an important area of China's development. This paper summarizes four research results of the Grassland Animal Husbandry Traceability Big Data Inner Mongolia Autonomous Region Engineering Laboratory by means of modern technologies such as artificial intelligence and Internet of Things.

References

1. Reference: a review on the use of sensors to monitor cattle jaw movements and behavior when grazing. [J] / Andriamandroso Andriamasinoro [et al.] // Biotechnologie, Agronomie, Société et Environnement. – 2016. – N 20 (7). – P. 141–145.
2. Implementation of an automatic 3D vision monitor for dairy cow locomotion in a commercial farm. [J] / Tom V. Hertem [et al.] // Biosystems Engineering. – 2018. – N 173 (14). – P. 166–175.
3. .Stakeholder Perceptions of Climate Extremes'Effects on Management of Protected Grasslands in a Central European Area. [J] / Malatinszky Ákos // Weather Climate and Society. – 2016. – N 8 (3). – P. 209–217.
4. 李倩. 基于深度学习的草地产草量预测方法研究. [D]. – 内蒙古科技大学, 2022.
5. Niedźwiecki, M. System identification based approach to dynamic weighing revisited. [J] / M. Niedźwiecki, M. Meller, P. Pietrzak // Mechanical Systems and Signal Processing. – 2016. – N 80. – P. 582–599.
6. 陈凯东, 杜永兴, 周李涌, 肖俊生,李宝山. 羊群无感知体重监测系统的设计. [J].– 黑龙江畜-牧兽医, 2022.
7. Individual identification of dairy cows based on deep learning and feature fusion. [J] / Y. Du [et al.] // Animal Science Journal. – 2022. – N 93 (1). – P. 13789.
8. Individual identification of dairy cows based on convolutional neural networks. [J] / W. Shen [et al.] // Multimedia Tools and Applications. – 2020. – N 79. – P. 14711–14724.

STUDIES ON VORTEX SAR IMAGING ALGORITHMS

Xiao Tang, Yong Xing Du, Zong Jun Tong

Inner Mongolia university of science and technology, China

Supervisor Yong Xing Du

Vortex electromagnetic waves carrying orbital angular momentum (OAM) have a spiral phase wave front and can be used to obtain more dimensional information in radar imaging. The introduction of vortex electromagnetic waves into synthetic aperture radar (SAR) imaging can break the traditional SAR imaging performance bottleneck problem and obtain higher resolution SAR imaging imagesvedvortex SAR imaging.

Keywords: orbital angular momentum, vortex electromagnetic waves, SAR imaging, BP algorithm, CS algorithm.

Introduction. Synthetic aperture radar (SAR) imaging is an all-day, all-weather radar imaging technology that can obtain good two-dimensional focused images in a variety of scenarios [1]. However, with the increase of people's requirements for radar imaging resolution, the resolution of traditional SAR imaging technology has been increasingly unable to meet the demand for high-resolution imaging images [2], so it is necessary to break through the bottleneck of traditional SAR imaging technology and carry out ultra-high resolution SAR imaging technology.

Orbital angular momentum (OAM) is an inherent property of electromagnetic waves, and electromagnetic waves are called vortex electromagnetic waves because they carry OAM and have a spiral phase wavefront [3]. The OAM has a theoretically infinite number of mutually orthogonal modes, so that more information can be modulated on the OAM [4]. The introduction of vortex electromagnetic waves into SAR imaging can obtain azimuthal high resolution [5], which provides a new idea to break through the bottleneck of traditional SAR imaging technology to achieve ultra-high resolution SAR imaging.

This paper analyzes the improved BP algorithm, which can adapt to vortex electromagnetic waves and compare the simulation results of vortex SAR imaging based on CS algorithm, and finds that the improved BP algorithm can solve the problem that vortex SAR imaging gradually scatters in azimuth as the modal number increases.

CS algorithm and improved BP algorithm

CS based Vortex SAR Imaging. Figure 1 shows a vortex SAR imaging model using a UCA transmitting an LFM signal with the radar mounted on the aircraft operating in side-looking strip mode. Let the origin of the coordinates be the centre of the trajectory of the carrier aircraft, and H be the altitude of the carrier aircraft, flying at a uniform velocity v along the x-axis, with the z-axis perpendicular to the xoy plane downwards.

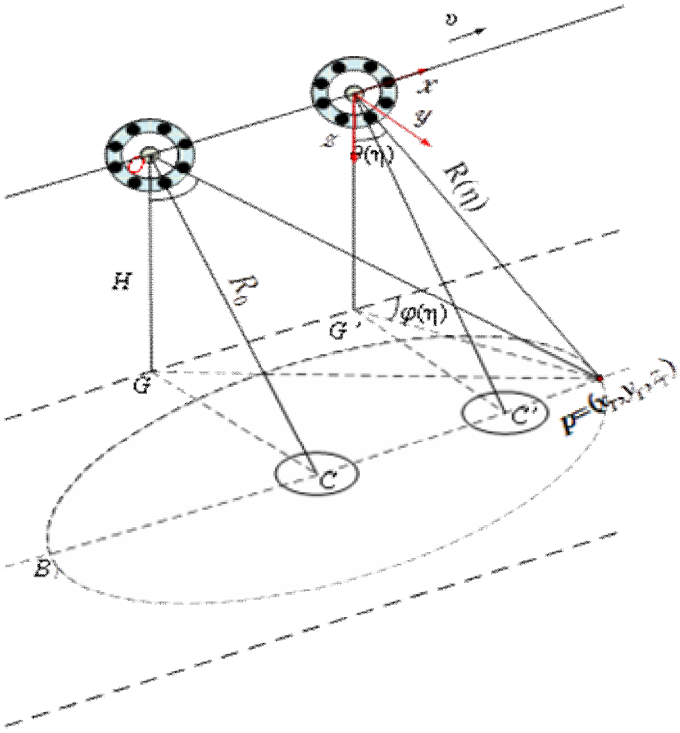

Fig. 1. Vortex imaging model

The echo signal received at point ρ can be expressed as:

$$
\begin{aligned}
s_{rp}(\tau, t, l) \approx \sigma N^2 \exp(jl\pi) w_r\left(t - \frac{2r(\tau)}{c}\right) w_a(\tau - \tau_c); \\
\exp\left(\frac{-j4\pi f_c r(\tau)}{c}\right); \\
\exp\left(j\pi K_r (t - \frac{2r(\tau)}{c}\right)^2; \\
\mathrm{J}_l^2\left[ka\sin\theta(\tau)\right]\exp\left(j2l\varphi(\tau)\right).
\end{aligned}
\tag{1}
$$

In equation (1) σ is the scattering area of the radar; a is the radius of the UCA antenna; t is the distance time; τ is the azimuthal time; K_r is the azimuthal tuning frequency; $r(\tau)$ is the distance slope; f_c is the antenna carrier frequency; l is the OAM mode number; c is the speed of light; $w_r(\bullet)$ and $w_a(\bullet)$ are the distance envelope and azimuthal envelope respectively; $J_l(\bullet)$ is the type I Bessel function; $k = 2\pi/\lambda$ is the wave number; $\tau_c = x/v$.

Azimuth and pitch angles can be obtained from geometric relationships:

$$
\begin{aligned}
\theta(\tau) = \arccos\left(\frac{H}{r(\tau)}\right); \\
\varphi(\tau) = \arccos\left(\frac{x - v\tau}{r(\tau)\sin\theta(\tau)}\right).
\end{aligned}
\tag{2}
$$

The algorithm flow chart for CS is consistent with the traditional CS algorithm. The simulation parameters and simulation results are shown in Table 1 and Fig. 2, respectively.

Table 1

Key simulation parameters of CS algorithm

Parameters	Value
Radar operating frequency f_c, GHz	9.6
flight speed v, (ms^{-1})	150
UCA Antenna radius a	30 λ
slant-range r, m	3400
Maximum number of modes in OAM	15
flight height H, m	2000
Chirp pulse band width, MHz	24
sampling frequency, MHz	98
Antenna center Angle, (°)	54
pulse repetition rate, HZ	300

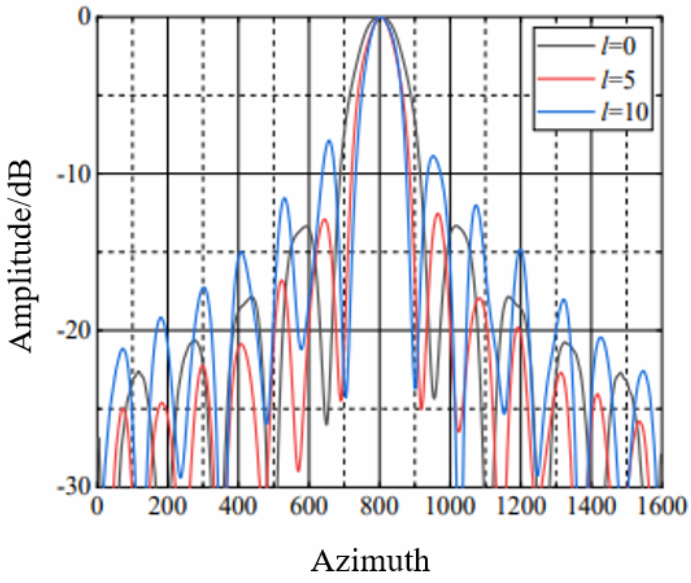

Fig. 2. CS algorithm azimuth profile

The simulation results show that as the number of modes increases, the azimuthal resolution increases and so does the azimuthal bypass level, with scattered focus occurring when the number of modes is large.

Improved BP algorithm. The flow chart of the improved BP algorithm is shown in Fig. 3. The phase compensation of the conventional BP algorithm is followed by a new azimuth matching filter $H_1(f_\tau, l)$ to compensate for the effect of OAM on the azimuth phase, and an azimuth amplitude filter $H_2(f_\tau)$ to compensate for the azimuth envelope to reduce the side flaps.

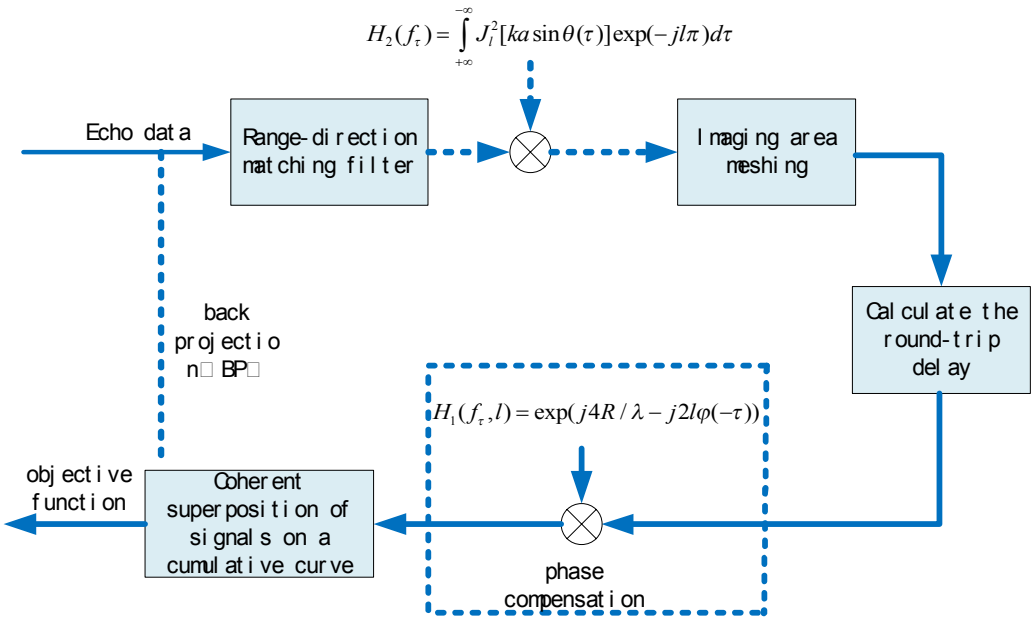

Fig. 3. Improved multi-mode EMV-SARBP algorithm

Table 2 shows the key simulation parameters used for the simulation.

Table 2

Key simulation parameters

Parameters	Value
Radar operating frequency f_c, GHz	5.3
flight speed v, (ms^{-1})	150
UCA Antenna radius a	30λ
slant-range r, m	3400
Range modulation frequency K_r, (Hzs^{-1})	20 × 1012
The time width of the transmitted pulse T_r, us	2.5
Sampling frequency in the range direction F_{sr}, MHz	60
pulse repetition rate PRF, Hz	100
Beam squint Angle $\theta_{r.c}$, (°)	3.5
angle of incidence β, (°)	67
UCA Number of antenna elements N	10
OAM Pattern number range Δl	[–4, 4]

The simulation results are shown in Fig.4:

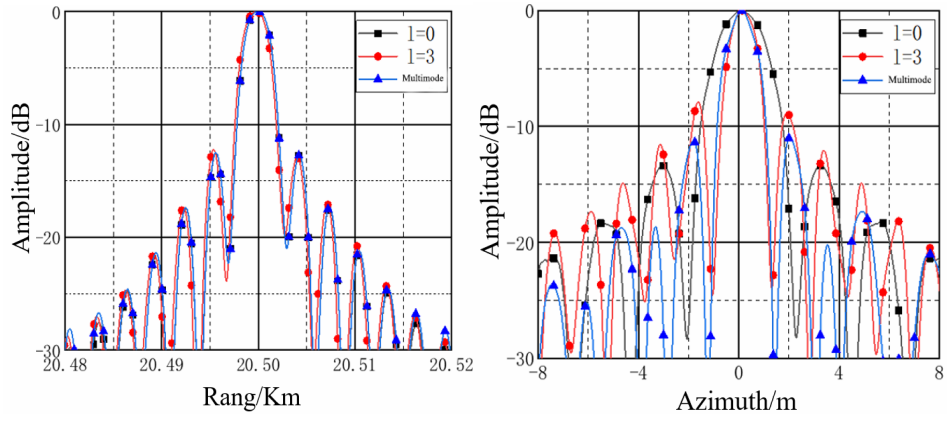

Fig. 4. A profile of the point target result

Analysis of the simulation results shows that as the number of modes increases, the distance-to-envelope remains almost unchanged and the azimuthal resolution increases. Because of the azimuthal amplitude filter, the azimuthal bypass level does not increase as much as the CS algorithm because of the increase in the number of modes.

Conclusion. Compared with conventional SAR imaging, scroll SAR imaging can achieve better azimuthal resolution, which can break through the bottleneck of conventional SAR imaging and become one of the directions to achieve ultra-high resolution, providing ideas for the development of new system radar in the future.

R e f e r e n c e s

1. Oliver, C. Understanding synthetic aperture radar images. [M] / C. Oliver, S. Quegan. – SciTech Publishing, 2004.
2. Very-high-resolution airborne synthetic aperture radar imaging: Signal processing and applications. [J] / A. Reigber [et al.] // Proceedings of the IEEE. – 2012. – N 101 (3). – P. 759–783.
3. Orbital-Angular-Momentum-Based Electromagnetic Vortex Imaging. [J] / K. Liu [et al.] // Ieee Antennas And Wireless Propagation Letters. – 2015. – N 14. – P. 711–714.
4. Encoding many channels on the same frequency through radio vorticity: first experimental test. [J] / F. Tamburini [et al.] // New journal of physics. – 2012. – N 14 (3). – P. 033001.
5. Implementation of vortex electromagnetic waves high-resolution synthetic aperture radar imaging. [J] / X. Bu [et al.] // IEEE antennas and wireless propagation letters. – 2018. – N 17 (5). – P. 764–767.